Bridging cumulative and noncumulative geometric frustration response via a frustrated N-state spin system

Snir Meiri and Efi Efrati *

Department of Physics of Complex Systems, Weizmann Institute of Science, Rehovot 76100, Israel

(Received 28 March 2022; revised 18 May 2022; accepted 29 June 2022; published 8 August 2022)

The resolution of geometric frustration in systems with continuous degrees of freedom often involves a cooperative inhomogeneous response and superextensive energy scaling. In contrast, the frustration in frustrated Ising-like spin systems is resolved uniformly. In this work we bridge between these two extremes by studying a frustrated model composed of N-state spins, and varying N. The expected cooperative response, observed for large N, is strongly attenuated as N is reduced, in a nontrivial way. Moderate N values show unique topological-like phases not observed before in frustrated models.

DOI: 10.1103/PhysRevResearch.4.033104

I. INTRODUCTION

Geometric frustration arises whenever the short-range interactions between the constituents of a system favor the formation of local motifs that are incompatible with long-range propagation in the ambient space geometry or topology. Examples of geometrically frustrated assemblies include: frustrated spin models [1–4] in which the frustration arises from a locally preferred misalignment of adjacent spins that cannot be reconciled over extended areas, and liquid crystals in which local tendencies of the constituents, such as a positive bend and vanishing splay and twist, necessitate the existence of unfavorable spatial structural gradients [5–8]. As the locally favored arrangement of the constituents cannot be realized, any finite assembly must exhibit some compromise of these locally favored tendencies. In some cases, such as the Ising antiferromanet on a triangular lattice, this unavoidable compromise can be made uniform, i.e., distribute the frustration energy evenly by incorporating a single unfavorable bond in every facet. Consequently, the energy associated with this compromise will grow extensively, proportional to the number of facets. Such frustration was recently termed noncumulative [9], in contrast with systems exhibiting cumulative frustration, such as the frustrated XY-model [10]. In the later model the optimal compromise in a single triangular facet precludes repeating the same compromise verbatim in the adjacent facets. As a result, the energy associated with the compromise in systems exhibiting cumulative frustration grows superextensively, and the ground state shows long-range cooperativity and depends on global properties of the system such as its aspect ratio and its spatial extent. The superextensive energy scaling and its dependence on global parameters may lead to growth arrest [11], the formation of filamentous structures [12,13], and give rise to exotic response properties [14,15]. Naturally, the superextensive energy scaling does not persist indefinitely and only applies to finite systems. Different types of geometric frustration may exhibit distinct mechanisms for frustration saturation for large systems, and in particular, could result in infinite bulks of extensive energy, defect ridden structures, or growth arrest along one or a few dimensions [7].

Considering moderately sized frustrated systems [16], in which the discrete degrees of freedom (DOF) may assume a very large number of states N, we expect to recover the continuous behavior that results in cumulative frustration. In contrast, as was recently shown, low N values lead to a local and uniform resolution of the frustration, saturating at the level of a single or a few facets [17]. The present work aims to understand this discrepancy by filling in the gap between these two distinct and limiting behaviors. By varying the granularity of the model in a controllable way, we identify the threshold value of the number of DOF leading to the loss of uniformity and the incorporation of spatial gradients to the system and relate its value to the frustration. We show that as N is increased the approach to the cumulative behavior is nonmonotonous and report a previously undescribed topological-like phenomena at intermediate granularity.

II. MODEL

We consider a frustrated N-state spin model, inspired by bent-core liquid crystals in which the frustrated behavior is well understood [6,10]. The basic components of the model, located on the vertices of a triangular lattice, are Potts-like spins that can be oriented along N equally spaced orientations in the plane. The interactions of the spins are set to favor slight misalignment according to the following Hamiltonian:

$$\mathcal{H} = \frac{1}{2}\sum_{\text{facets}} K_1\Psi_1^2 + K_3(\Psi_2 - b_0)^2, \tag{1}$$

*efi.efrati@weizmann.ac.il

Published by the American Physical Society under the terms of the Creative Commons Attribution 4.0 International license. Further distribution of this work must maintain attribution to the author(s) and the published article's title, journal citation, and DOI.

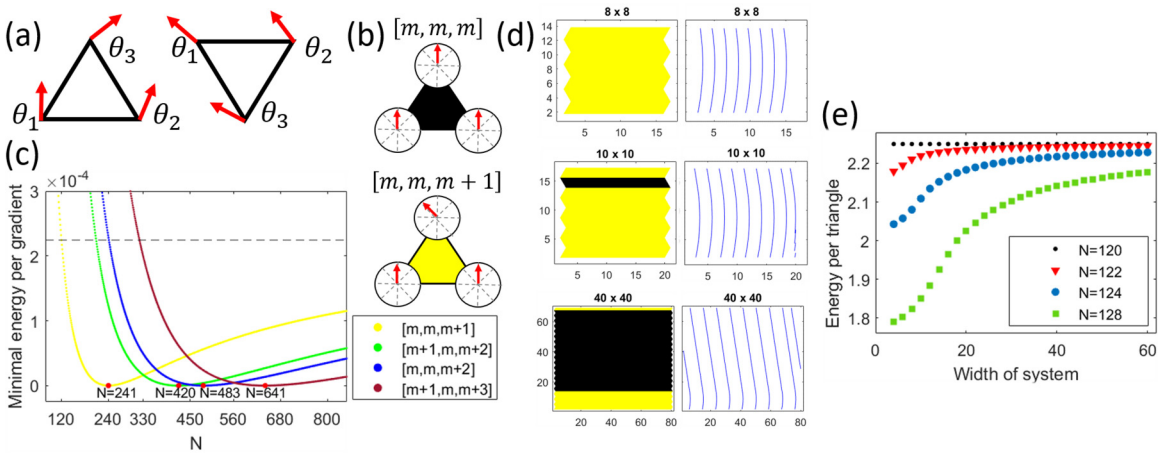

FIG. 1. (a) Notations of vertices of upright (left) and up-side-down (right) triangles. (b) Color coding of two possible conformations of the spins. The state key on top is defined such that each entry represents a state of a spin according to the notations in (a). m is any integer between 1 and N where N is the number of states in the model. (c) The minimal energy of a single triangle in a given conformation type for different N values. The N at which this minimal value is attained is marked. The dashed line marks the energy of the trivial constant solution. (d) Resulting minimal conformations for lattices of 8×8, 10×10, and 40×40 sites per edge in the case of $N = 124$. Color coding of the left panels is according to the gradient types in (b) and the right panels display the interpolated streamlines. (e) Energy per triangle vs. the width of the system (number of sites per edge) for different values of N near the cumulative-non-cumulative transition.

where $b_0 = \text{const.} \neq 0$, which has the dimensions of inverse length [18], is responsible for the frustration in the system, and the auxiliary variables Ψ_i can be computed directly from the spins in each facet according to

$$\Psi_1 = -\frac{\theta_2 - \theta_1}{l}\sin(\bar{\theta}) \pm \frac{2\theta_3 - \theta_2 - \theta_1}{\sqrt{3}l}\cos(\bar{\theta}),$$
$$\Psi_2 = \frac{\theta_2 - \theta_1}{l}\cos(\bar{\theta}) \pm \frac{2\theta_3 - \theta_2 - \theta_1}{\sqrt{3}l}\sin(\bar{\theta}), \qquad (2)$$

where $\bar{\theta} = (\theta_1 + \theta_2 + \theta_3)/3$ and the $+$ $(-)$ sign corresponds to upright (upsidedown) triangles, see Fig. 1(a).

In the limit $N \to \infty$ this model recovers the recently introduced frustrated XY-spin model [10] exhibiting cumulative frustration. In this limit the spin texture is interpreted as a director field and Ψ_1 and Ψ_2 are identified with the director's splay and bend fields, respectively, and b_0 may be interpreted as the reference bend value. For finite N values Ψ_1 and Ψ_2 may only assume a finite collection of states, which is further reduced by the discrete compatibility conditions. For more details regarding the manner in which this model is related to planar bent-core liquid crystals and regarding the response in the case of the frustrated XY-spin model see [10].

To probe the effects of discrete response modes on the frustrated conformations of minimal energy, the ground state of the system was approached numerically. Due to the highly coupled nature of the problem the stochastic sampling of individual spins proved inefficient, and at each simulation step a pair of edge-sharing spins were sampled. The numerical process included two rounds each comprised of a simulated annealing stage combined with a global step that probed the energetic benefit associated with the rigid rotation of domains of finite size in the system. While we cannot preclude the possibility that the obtained states reflect a local minimum of the energy rather than the (possibly degenerate) true ground state, these were obtained as the configurations of minimal energy starting from multiple initial conditions, and show relative continuity as both the granularity and the number of particles are varied. For more details see the Appendix. The chosen parameters are $K_1 = K_3 = 2$, edge length in the lattice of $l = 2$, and preferred misalignment of $b_0 = 0.015$. Free boundary conditions were used throughout the optimization process.

The spins of a given triangle in the lattice are ordered according to Fig. 1(a) and their states are expressed as $[m_1, m_2, m_3]$, where m_i are positive integers between 1 and N corresponding to their orientations. Note that throughout this work the local orientations are bounded away from both 0 and 2π, thus the periodicity of the angular variable does not come into play. To focus on the spatial gradients in the orientation we identify the minimal orientation value in each facet, $\min(m_i) = m$, and express the facet orientation as $[m + a, m + b, m + c]$ with a, b, and c nonnegative integers, at least one of which is zero. Each type of spatial gradient about m corresponds to a specific triplet (a, b, c) and is color-coded consistently throughout this paper.

III. ONSET OF NONUNIFORM TEXTURES

We first come to examine the threshold granularity $N = N_t$ below which it is unfavorable to introduce spatial gradients to the ground-state texture. Even for a single triangular facet, and the misalignment b_0, it is not always favorable to form any gradient of the orientations. The state $[m, m, m]$ represents the trivial constant solution, and the state $[m, m, m + 1]$ represents the smallest possible deviation from it (along with its permutations). Given a certain value of b_0, it might be unfavorable to form any type of nontrivial solution as the lowest possible deviation of the orientations is too large. For the above-mentioned parameters, the energetic cost of the trivial solution is $e = b_0^2$. The energetic cost of the smallest

deviation from it reads

$$e = b_0^2 + \frac{4\pi^2}{3N^2} - \frac{4\pi b_0}{\sqrt{3}N}\sin\left[\left(m+\frac{1}{3}\right)\frac{2\pi}{N}\right]. \quad (3)$$

This energy is favorable whenever

$$N > \frac{\pi}{\sqrt{3}b_0 \sin\left[\left(m+\frac{1}{3}\right)\frac{2\pi}{N}\right]} > \frac{\pi}{\sqrt{3}b_0}. \quad (4)$$

Setting $b_0 = 0.015$ we obtain $N_t > 120.91$. Note that any system whose diameter D includes many individual particles, i.e., $1 \ll D$, yet is smaller than the geometric lengthscale associated with the frustration $D < 1/b_0$ will require b_0 to be small, and consequently, $1 \ll N_t$. We return to this point in the discussion.

Figure 1(c) shows the optimal energy of a single facet versus N for several gradient types. One can see that the threshold at which the trivial solution, marked with a dashed line, ceases being the most favorable reads $N_t = 121$. Incorporating a deviation from a given orientation m may exclude repeating the same gradient type with the same m value in its vicinity. As the energy depends on the value of m the energetic cost of a uniform gradient in the system may vary spatially. The minimized conformations in the case of a marginal granularity of $N = 124$ is shown in Fig. 1(d). The uniform gradient causes the value of m to vary spatially, leading the gradient orientation to deviate away from the local average orientation and thus contribute to Ψ_1 rather than Ψ_2. By examining Eq. (3) we obtain that, for $N = 124$, only nine distinct values of m keep the deviation energy of the gradient $[m, m, m+1]$ smaller than the energy of the uniform phase b_0^2. As this gradient causes the value of m in adjacent lines to increase by 1 we conclude that large domains will only show nine lines of gradients, with the remainder of the domain showing the trivial solution. This result is general for marginal values of $N_t \lesssim N$, where the incorporation of gradients is favorable only in small domains up to a finite size. Further increasing the size of the system will incorporate only domains of trivial solution rendering the energetic signature of the nontrivial regions less distinguishable, as can be seen in Fig. 1(e).

IV. INCORPORATION OF MORE COMPLEX RESPONSE MODES FOR A MORE REFINED GRANULARITY

As the granularity of the orientation of the spins is reduced, by increasing N, more complex response modes are incorporated into the ground state. While marginal values of N only display uniform gradient ground states, i.e., the entire solution is comprised of a single gradient type $[m+a, m+b, m+c]$, for higher values of N nonuniform responses appear.

Figure 2 displays the representative samples of the ground-state solutions for $N = 356$ depicting the transition between gradient types as the domain size is increased. From Fig. 1(c) we deduce that for $N = 365$ the gradient $[m+1, m, m+2]$ is associated with the minimal energy for a single triangle, while the gradient $[m, m, m+1]$ is associated with the next lowest energy. Indeed, the ground state of the smallest domain in Fig. 2(a) displays only a single gradient $[m+1, m, m+2]$. Moreover, as depicted in Fig. 2(e), the energy associated with the uniform gradient $[m+1, m, m+2]$ increases very fast with system size, while the energy associated with the

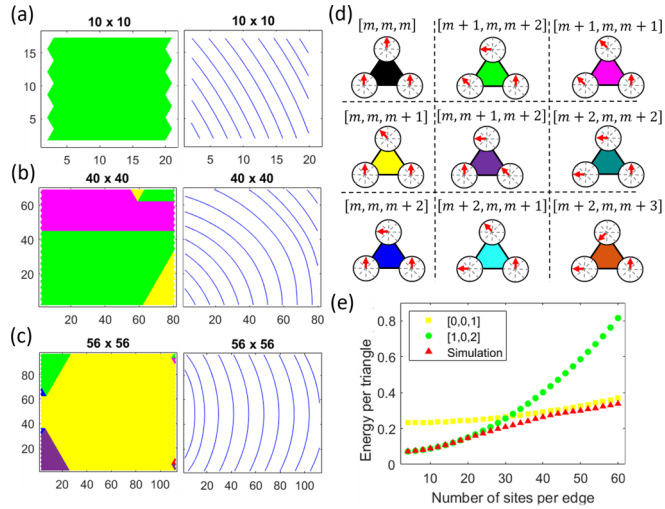

FIG. 2. Results for $N = 356$. (a)–(c) Resulting minimal conformations for lattices of 10×10, 40×40, and 56×56 sites per edge, respectively (note that as stated above $l = 2$). Color coding of the gradient types in the panels to the left is according to (d) and the right panels display the interpolated streamlines. (e) Energy per triangle vs. the number of sites per edge in isotropically growing lattices. The resulting conformations from the simulation marked in red triangles are shown together with the minimal energies per triangle in lattices of a single conformation where $[m, m, m+1]$ and $[m+1, m, m+2]$ are marked in yellow squares and green circles, respectively.

uniform gradient $[m, m, m+1]$ grows at a much slower rate. Consequently, for larger systems we expect the gradient type $[m, m, m+1]$ to dominate the ground-state solution, as seen in Fig. 2(c). Note that the transition is not abrupt and that the system succeeds in further lowering the elastic energy by incorporating additional gradient types. This behavior demonstrates the global aspects of cumulative geometric frustration, as the optimal solution for larger domains may be fundamentally different from the solutions for smaller domains.

As the value of N is further increased large domains display more intricate ground states. Figure 3 displays the ground state for three domain sizes for $N = 446$. Figure 3(a) shows a relatively small domain in which the ground state is given by the uniform gradient $[m+1, m, m+2]$, as predicted in Fig. 2(c) for a single triangle. Note, however, that while the gradient is uniform the energy is not; the local energy also depends on the relative orientation between the direction of the gradient and the average local orientation given by m. Figure 3(e) shows the dependence of the energy of a single triangular facet of nine gradient types on the local value of m. The energetically favorable gradient type for a certain m value may be succeeded by another gradient type as m is varied. In the constant gradient solution displayed in Fig. 3(a) the optimal m value is obtained along one of the diagonals of the domain. Away from this diagonal m varies, leading to the strain energy buildup in the top-left and bottom-right corners of the domain. Figure 3(b) show that, as the domain size is increased, the growing strain is screened by incorporating different gradient types in these energetically unfavorable regions, namely, $[m, m, m+2]$ and $[m+2, m, m+2]$. Note, however, that the discrete compatibility conditions preclude

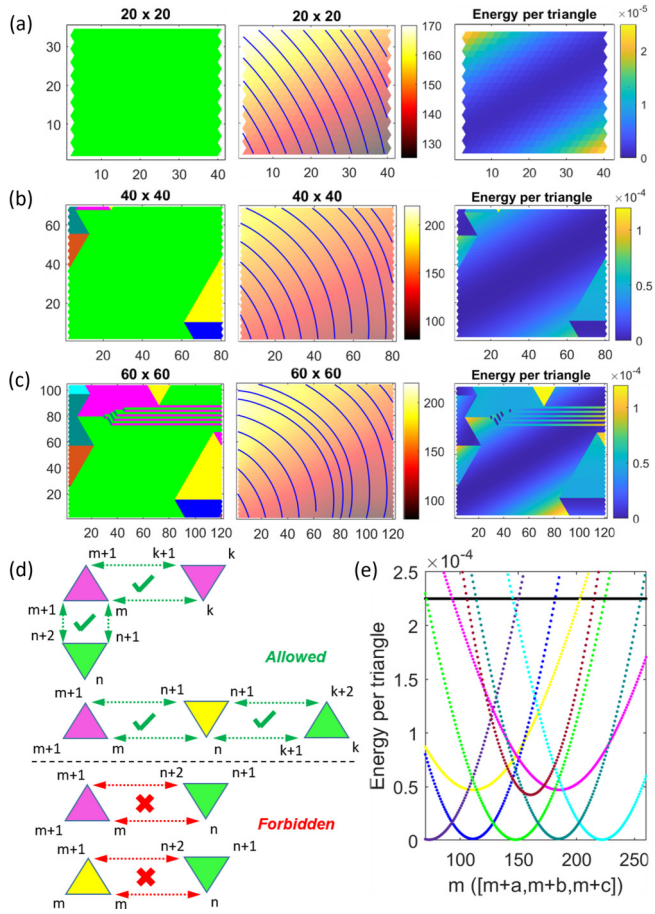

FIG. 3. Results for $N = 446$. (a)–(c) Resulting minimal conformations for lattices of (a) 20×20, (b) 40×40, and (c) 60×60 sites per edge. Color coding is according to Fig. 2(d). Each triplet shows gradient types (left), interpolated streamlines along with corresponding m value heat-map (middle) and energy per site (right). Notice different color-bar scales. (d) A graphic representation of the orientation-dependent allowed and forbidden transitions between gradient types. (e) Energy per a single triangle of a conformation $[m + a, m + b, m + c]$ vs. m in that notation. The color coding is also according to Fig. 2(d).

the gradient type $[m, m, m + 2]$ at the bottom right from having a horizontal or upper-right diagonal interfaces with the underlying $[m + 1, m, m + 2]$ gradient. Consequently, it must be buffered by an additional gradient type, $[m, m, m + 1]$ that bridges between the incompatible gradients. While the buffering gradient $[m, m, m + 1]$ is less energetically favorable, its presence is necessitated by the discrete compatibility conditions. In the upper-left corner of Fig. 3(b) we similarly observe the incorporation of a buffering gradient $[m + 2, m, m + 3]$ to bridge between two incompatible gradients.

Figure 3(c) depicts a further increase in domain size and the appearance of a more intricate texture. A new gradient type $[m + 1, m, m + 1]$(marked by the pink domain) is incorporated near the top-left portion of the domain to reduce the local stain. This gradient type, while allowing horizontal interfaces with the underlying $[m + 1, m, m + 2]$ gradient (marked in green), cannot share any diagonal interface with it. Consequently here too a buffering gradient is required. Growing the buffering gradient $[m, m, m + 1]$ (marked in yellow) along the entire incompatible interface is prohibitively energetically costly. As a result, the bottom region of the (pink) gradient $[m + 1, m, m + 1]$ must extend all the way to the boundary of the domain. This gives rise to the (pink) striped pattern in the upper-half of Fig. 3(c). These stripes, while energetically unfavorable compared to the background gradient, are required by the compatibility conditions to reach a boundary.

Frustrated systems with continuous DOF are characterized by their compatibility conditions restricting the realizable local structures [9]. In systems with discrete degrees of freedom these conditions are replaced by local matching rules between the states of adjacent sites. For a continuous two-dimensional unit vector field, the compatibility condition consists of a single partial differential equation relating the local bend and splay and their oriented first derivatives [6]. For the frustrated XY model on a triangular lattice the compatibility condition restricts the possible splay and bend values in any three side-sharing triangular facets [10]. In the present case, as our basic building blocks are oriented gradients we encounter a nearest-neighbor compatibility condition in the form of a local restrictions rule prescribing the gradients that are allowed to share a (specific) edge with a given gradient as depicted in Fig. 3(d). In addition, the discrete analog of the continuous compatibility condition predicts uniquely the gradient of a facet given the gradients in two of its side sharing triangular facets.

For moderate N values, where the state space of the system is limited, the system may seek to incorporate mismatching states next to one another. In such cases, energetically unfavorable buffering domains [as depicted in Fig. 3(b)] will form. As the energetic cost of these buffering domains becomes exceedingly large the mismatched domains will be topologically required to span the entire system to the free boundary, as in Fig. 3(c).

V. SUPEREXTENSIVE ENERGY SCALING AS A FUNCTION OF N

Considering the energy scaling with system size we observe the expected transition from a uniform resolution of the frustration at low N values to a highly cooperative ground states exhibiting a superextensive energy scaling at large N values. Large-enough N values recover quantitatively the behavior of the corresponding continuous frustrated XY-spin system where the energy per particle scales as $E/A \propto A$, where A is the area of the system [10]. Figure 4 shows that for $N = 8192$ the system follows closely the superextensive energy scaling of the continuous case, while the system at $N = 120$ follows an extensive energy scaling. The transition between these two limiting behaviors is, however, nonmonotonic. For example, while $N = 128$ follows closely the extensive scaling, $N = 240$ displays a superextensive scaling quite similar to the continuous case, and $N = 330$ again shows only small deviations from an extensive behavior. One may expect that, as N is increased, more refined gradients could be constructed to better approximate the continuous case; this is indeed the case for large N values. For moderate N-values, however, "resonant"-like values of N could approximate the attempted gradient b_0 almost perfectly, while

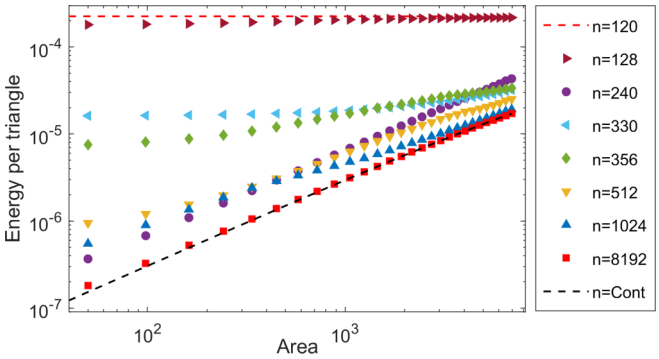

FIG. 4. Logarithmic plot of the energy per triangle of the ground states resulting from the simulation vs. the area of isotropic domains for different directions granularity values N. The black dashed line (bottom) shows the results in the case of the continuous XY spins, as was presented in [10].

nearby increased values such as $N+1$ will not perform as well. These discrete effects, most prominently manifest for moderate N-values also affect the compatibility conditions and the rate at which the energy of a given gradient varies as m is varied. As the resonant mechanism responsible for the nonmonotonous approach to the continuum limit is general, we expect this phenomenon to appear in other frustrated systems at moderate levels of granularity.

VI. DISCUSSION

The frustrated N-state spin model presented here allows us to bridge the gap between the cumulative frustration of the frustrated XY-model, and the noncumulative frustration of the Ising antiferromagnet on a triangular lattice. Up to $N_t = 121$ all the spins in the ground state are coaligned, and the ground-state energy is extensive. The threshold value N_t is inversely proportional to the relatively small strength of the frustration $b_0 l \ll 1$. While increasing b_0 may lower N_t, it also decreases the lengthscale associated with the geometric frustration and thus diminishes the domain size at which frustration saturation is met. Eventually, when the geometric lengthscale associated with the frustration becomes shorter than a single unit cell, no characteristics of the cumulative frustration will remain [9].

For large values of N the cumulative frustration behavior of the continuum limit is recovered and the granularity of the DOF does not play a significant role in shaping the ground state. However, for moderate values of N, while we observe cumulative frustration and a highly cooperative ground state, the discrete nature of the DOF leads to qualitatively different ground states and exotic response properties that are not observed in the continuous case. These include the formation of striped patterns and the appearance of buffering moderate energy regions that facilitate the incorporation of low-energy domains whose incorporation is otherwise precluded by the discrete matching rules. These motifs are unique to the discrete-frustrated-spin system and have no analog in the continuous frustrated XY-model.

ACKNOWLEDGMENT

This work was funded by the Israel Science Foundation Grant No. 1444/21.

APPENDIX: DESCRIPTION OF THE NUMERICAL SCHEME

The numerical scheme implemented in this work consists of two iterations of a simulated annealing cycle. The strong energy coupling between edge sharing facets results in significant energy barriers. Consequently, single spin variations are generally unfavorable even in high-energy configurations. To circumvent this difficulty at every time step the value of an edge-sharing spin pair is probed.

Spin orientation values are varied by single steps, i.e., for a spin at the state m, the scheme only considers the adjacent states $m-1, m, m+1$. Throughout the process all spin orientations are far from 0 and 2π, thus we need not address comparing spin values across the orientation discontinuity. For every spin pair chosen, each of the nine possible adjacent states is examined and its energy variation Δ_i is computed. The resulting state i is drawn from the probability $e^{-\frac{\Delta_i}{T}} / \sum_{k=1}^{9} e^{-\frac{\Delta_k}{T}}$, where T is the temperature at the step.

The states obtained from the numerical minimization of the energy show a high degree of cooperativity. Up to $N = N_t = 121$ the ground state of the system displays no gradients. For $N = 446$ Fig. 3(a) shows a single gradient type, yet a spatially varying energy density that results from the spatial variation in m. The most favorable m-value for the realized gradient type is realized in the center of the domain and approximately along one of the main diagonals of the domain. The underlying uniform gradient dictates how the value of m changes spatially. There are many such distinct states sharing the same uniform gradient, yet differing in their m values. Some could possibly be of lower energy, yet transitioning between these states by varying the local spin pairs would inevitably create a large interface of an unfavorable gradient type. Such prominent energy barriers are characteristic of low-moderate N values. As N is increased the incorporation of additional gradients (though which the system could gradually vary its state) becomes energetically cheaper and more prevalent. To overcome such a barrier we incorporate a step of exploration of global transformations in which the spins in the entire domain are simultaneously rotated, keeping the gradients unaltered.

As the domain size considered is increased the numerical minimization resulted in states divided to subdomains, in each of which the gradients were uniform. To verify that the boundaries between these domains are not trapped kinetically away from their optimal position we part the domain by a single straight line (along one of the systems natural directions) into two subdomains and explore their independent uniform rotations.

The exploration of these two types of global transformations is preceded by a simulated annealing stage and followed by another annealing stage. The results presented in this work are obtained by repeating such a cycle twice.

Each cycle starts with an annealing stage separated to a faster stage at which the temperature is lowered linearly from from $T = T_{\text{initial}}$ to $T = 0.3$ ($T_{\text{initial}} = 2$ for the first round and $T_{\text{initial}} = 1$ for the second round) at equal decrements over the number of steps given by $n_{\text{Iter},1} = n_{\text{Sites}} \times \max(400, N)$, where, as in the main text, N denotes the spin's number of states. At the second stage of annealing the rate is slowed and the temperature reduction proceeds over $n_{\text{Iter},2} = n_{\text{Sites}} \times$

$\max(900, 2.25 * N)$ time steps. As a single step before reaching vanishing temperature the annealing is stopped and global transformations are explored and accepted if they lead to a reduction in energy. The global transformations include varying all spin values by uniformly rotating them by $-16 \leqslant \delta \leqslant 16$ steps (For low N values this was reduced to $-N/20 \leqslant \delta \leqslant N/20$). In addition, sectioning the system by a single horizontal, diagonal, or vertical line and assigning distinct uniform rotations in the two domains is explored. A third phase of annealing is performed next, consisting of $n_{\mathrm{Iter},3} = \lfloor \frac{n_{\mathrm{Iter},2}}{3} \rfloor$ steps with temperature decrements of $dT_3 = \frac{T_{\mathrm{Ini},3}}{n_{\mathrm{Iter},2}+1}$, where $T_{\mathrm{Ini},3}$ is the temperature at the beginning of the stage, which coincides with the temperature of the last step of the preceding annealing stage.

[1] G. H. Wannier, Antiferromagnetism the triangular ising net, Phys. Rev. **79**, 357 (1950).

[2] S. Teitel and C. Jayaprakash, Josephson-Junction Arrays in Transverse Magnetic Fields, Phys. Rev. Lett. **51**, 1999 (1983).

[3] T. C. Halsey, Josephson-junction arrays in transverse magnetic fields: Ground states and critical currents, Phys. Rev. B **31**, 5728 (1985).

[4] M. Lankhorst, A. Brinkman, H. Hilgenkamp, N. Poccia, and A. Golubov, Annealed low energy states in frustrated large square josephson junction arrays, Condensed Matter **3**, 19 (2018).

[5] R. B. Meyer, Structural problems in liquid crystal physics, *in Molecular Fluids*, edited by R. Balian and G. Weill, Proceedings of the Les Houches Summer School of Theoretical Physics 1973 (Gordon and Breach, New York 1976).

[6] I. Niv and E. Efrati, Geometric frustration and compatibility conditions for two-dimensional director fields, Soft Matter **14**, 424, (2018).

[7] M. F. Hagan and G. M. Grason, Equilibrium mechanisms of self-limiting assembly, Rev. Mod. Phys. **93**, 025008 (2021).

[8] J. V. Selinger, Director deformations, geometric frustration, and modulated phases in liquid crystals, Annu. Rev. Condens. Matter Phys. **13**, 49 (2022).

[9] S. Meiri and E. Efrati, Cumulative geometric frustration in physical assemblies, Phys. Rev. E **104**, 054601 (2021).

[10] S. Meiri and E. Efrati, Cumulative geometric frustration and superextensive energy scaling in a nonlinear classical XY-spin model, Phys. Rev. E **105**, 024703 (2022).

[11] B. Tyukodi, F. Mohajerani, D. M. Hall, G. M. Grason, and M. F. Hagan, Thermodynamic size control in curvature-frustrated tubules: Self-limitation with open boundaries, ACS Nano **16**, 9077 (2022).

[12] G. Meng, J. Paulose, D. R. Nelson, and V. N. Manoharan, Elastic instability of a crystal growing on a curved surface, Science **343**, 634 (2014).

[13] M. Lenz and T. A. Witten, Geometrical frustration yields fibre formation in self-assembly, Nat. Phys. **13**, 1100 (2017).

[14] K. Sun and X. Mao, Fractional Excitations in Non-Euclidean Elastic Plates, Phys. Rev. Lett. **127**, 098001 (2021).

[15] I. Levin and E. Sharon, Anomalously Soft Non-Euclidean Springs, Phys. Rev. Lett. **116**, 035502 (2016).

[16] Much larger than the scale of the constituents yet smaller than the typical geometric scale associated with the frustration, which in the present case reads $1/b_0$.

[17] P. Ronceray and B. Le Floch, Range of geometrical frustration in lattice spin models, Phys. Rev. E **100**, 052150 (2019).

[18] Compared with the length of an edge in the lattice l.